PAPER

Damage localization in fiberglass-reinforced composites using laser induced graphene

IOP Publishing Smart Materials and Structures
Smart Mater. Struct. **30** (2021) 035006 (11pp) https://doi.org/10.1088/1361-665X/abdc0c

Damage localization in fiberglass-reinforced composites using laser induced graphene

LoriAnne Groo[1], Jalal Nasser[1], Daniel Inman[1] and Henry Sodano[1,2,3]

[1] Department of Aerospace Engineering, University of Michigan, Ann Arbor, MI 48109, United States of America
[2] Department of Macromolecular Science and Engineering, University of Michigan, Ann Arbor, MI 48109, United States of America
[3] Department of Materials Science and Engineering, University of Michigan, Ann Arbor, MI 48109, United States of America

E-mail: hsodano@umich.edu

Received 12 November 2020, revised 21 December 2020
Accepted for publication 14 January 2021
Published 2 February 2021

Abstract

Current *in situ* piezoresistive damage detection techniques for fiberglass-reinforced composites are limited in widespread application as they require complex processing techniques which inhibit the scalability of the methods. To eradicate such challenges and expand the use of piezoresistive monitoring of fiberglass composites, this work utilizes a simple, scalable process to coat electrically insulating commercial fiberglass prepreg with piezoresistive laser induced graphene (LIG) for the detection and localization of damage. Recently, LIG has attracted substantial research attention due to the simplicity of the methodology and the piezoresistance of the LIG. Here, the LIG is transfer printed onto commercial fiberglass prepreg which is subsequently used to localize damage in all three dimensions of the resultant fiberglass-reinforced composites while also maintaining the structural properties of the composites. A combination of *in situ* and ex-situ resistance measurements are used to accomplish this objective: First, *in situ* measurements are used to determine the relative location of damage in one-dimension under tensile loading. Subsequently, separate *in situ* measurements are used to locate damage through the thickness under flexural loading. Finally, ex-situ methods are used to calculate the two-dimensional location of a hole in a plate. The LIG is found to reliably and accurately localize the damage to the composite in each case thus demonstrating for the first time that transfer printed LIG enables self-sensing of damage location in fiberglass composites. The result of this work is thus a multifunctional material capable of locating damage in all three-dimensions which is notably fabricated using commercial materials and scalable methodology.

Keywords: laser induced graphene, piezoresistance, damage localization, fiberglass composites

(Some figures may appear in colour only in the online journal)

1. Introduction

Continuous fiber-reinforced polymer matrix composites are extensively found in structures where high strength to weight ratio materials are desirable, such as aircraft and automobiles. As a result of the dynamic environments the material is subjected to in these applications, fiber-reinforced composites experience combined loading that can result in several failure types including fiber-matrix debonding, inter-ply delamination, matrix cracking, fiber failure, or any combination of these failure modes. Since these types of damage in laminar composites can lead to catastrophic failure of the structure

or component, knowledge of the current state of the material is critical for the safety and reliability of such structures while in service. Currently, composite structures under high and dynamic loading environments, such as aircraft, are removed from service and inspected for damage or deterioration using non-destructive evaluation which is expensive, labor-intensive, and time consuming. As an alternative to the currently employed damage detection methods, multiple structural health monitoring (SHM) approaches have been proposed to detect and localize damage *in situ* in fiber reinforced composites. Among the most common techniques which have been experimentally investigated are acoustic emission testing (AET) [1–8] and resistance-based sensing [2, 3, 9–12].

AET uses the release of elastic energy during the occurrence of damage to assess when damage occurs. Most commonly, piezoelectric materials have been used to sense the propagating lamb waves released during damage [7, 8, 13–15], but as a more recent alternative, less invasive fiber Bragg grating sensors have also been shown to be equally effective [16–18]. With a knowledge of the location of the sensors along the structure, a system or combination of AET measurements can be used to localize the damage by using differences in the time of arrival of the propagating wave at different sensors. However, this approach requires a knowledge of the wave propagation velocity and attenuation to perform the necessary calculations [6]. In the case of fiber-reinforced composites, the anisotropic nature of the material increases the complexity of this localization method, and thus limits the accuracy of damage location prediction in these materials following the time-of-arrival approach [19–21]. Furthermore, localization is achieved using complex networks of sensors that are either externally bonded or discretely embedded within the composite under investigation. This methodology is therefore limited by surface condition requirements for external bonding, and the potential for increased risk of delamination due to the addition of sensors or additional fibers, which have a diameter independent of that of the reinforcing fiber of the composite, in the interlaminar portion of the composite. Moreover, given the nature of the detection mechanism, AET is only capable of detecting damage *in situ* and is not designed for the monitoring and tracking of damage after its occurrence, thus limiting its effectiveness. Additionally, for comparison of wave attenuation and wave time-of-arrival comparisons, the described sensors require a certain orientation or proximity relative to the damage source [6, 16]. In summary, although AET can be useful in detecting and localizing damage in certain materials and structural applications, an improved method with a fully integrated sensing component for both *in situ* and retroactive damage localization in fiberglass reinforced composites is needed for the widespread use of SHM.

Resistance-based damage detection has been widely investigated for multiple fiber reinforcements, the most common of which are carbon and fiberglass [9–11, 22–24]. Due to the inherent piezoresistivity of carbon fiber, carbon fiber reinforced composites are capable of self-sensing damage location *in situ* and ex-situ by monitoring local changes in conductivity using multiple resistance measurements. As damage occurs to the composite or fibers, some carbon–carbon contacts are broken resulting in a decrease in conductivity in the area of the damage. In contrast, in the case of an electrically insulating reinforcing fiber, such as glass, an added conductive element is needed for resistance-based strain and damage monitoring. Multiple conductive nanomaterials have been investigated as matrix inclusions or surface coatings along the reinforcing fibers of fiberglass reinforced polymer composites, the most common of which include graphene oxide and carbon nanotubes (CNTs) [22, 25, 26]. Similar to the methodology used for conductive carbon fiber composites, once damage occurs to the fiberglass reinforced composites containing conductive nanofillers, local separations between conductive nanofillers result in a detectable decrease in conductivity. By taking multiple measurements at various locations on the composite, relative changes in conductivity can be used to locate the damage using either the electrical potential method or electrical impedance tomography (EIT) [12, 27–29]. The electrical potential method relies on local changes in impedance while EIT is more complex in execution and is used to reconstruct the local conductivity of the specimen under investigation and more precisely locate the points of conductivity change [30]. For example, Gallo *et al* used both the normalized resistance change approach and EIT to locate damage in two-dimensions in a fiberglass plate with embedded CNTs and provides a comparison between the two methods [29]. However, although effective, CNTs pose processing challenges such as increased viscosity of the uncured matrix and issues with agglomeration due to van der Waals forces [31], which decrease the translatability to the large scale fabrication of composite structures. Thus, a scalable, low-cost, and automatable alternative is desired for increased use of resistance-based SHM and damage localization in fiberglass reinforced composites, particularly for large scale industrial components.

Laser induced graphene (LIG) [32] has recently received significant research attention due to the simplicity and scalability of the synthesis methodology, in addition to the excellent properties which have expansive potential applications including microsupercapacitors [33–35], biological sensors [36, 37], and flexible strain sensors [38–40] among others. LIG is formed by irradiating polyimide using a commercial pulsed CO_2 infrared laser in an ambient environment, resulting in a tailorable, porous graphene nanostructure which is obtained using highly automatable techniques and commercially available materials [32]. Due to its graphitic composition, LIG is found to be inherently piezoresistive [36, 38–40], making it an excellent candidate for damage self-sensing applications using common resistance monitoring methods. For example, recent work has explored transfer printed LIG on fiberglass prepreg for *in situ* sensing of composite strain and damage using a four-probe resistance measurement technique [41]. The composites with integrated LIG were shown to be sensitive to both flexural and tensile loading and resulted in significant changes in conductivity which correlated to the occurrence of damage within the test specimens. It was observed that as the fiberglass composites with LIG experienced strain, small microcracks or gaps formed within the microstructure of the LIG thus leading to an increase in measured resistance. As the

composite strain increased and the host composite experienced damage such as in the form of delamination or fiber fracture, corresponding separations within the conductive carbon–carbon contacts within the integrated LIG interlayers resulted in sudden increases in the measured resistance [41]. To further exploit the piezoresistance of LIG for SHM, the research described here combines resistance-based damage localization with the ease and scalability of LIG for the *in situ* and ex-situ localization of damage in fiberglass reinforced composites. Fiberglass reinforced composites with integrated LIG are fabricated using a two-step transfer-printing process, after which three separate sets of mechanical tests are completed to evaluate the ability of the composite to localize damage in three dimensions. First, the damage is localized along the length of sample beams during tensile testing, after which the damage is localized through the thickness of the composite under flexural loading using a three-point bend test, and finally, damage in the form of a through-hole is localized in the two-dimensional plane of the composite. Thus, for the first time, this work investigates the potential for LIG to be used for three-dimensional damage localization in fiberglass composites. This work thus advances the state of the art by utilizing novel multifunctional LIG for localization of damage in three dimensions in fiberglass-reinforced composites.

2. Materials and methods

2.1. LIG and composite fabrication

LIG was coated onto the surface of the fiberglass prepreg using a two-step transfer printing process highly conducive to scaled-up roll-to-roll processing. First, commercial polyimide tape (2 mil Kapton®) was irradiated using a 60 W CO_2 laser (Epilog Zing 16 universal laser system) as illustrated in the schematic in figure 1(a). It should be noted that the polyimide tape acts as a precursor for the LIG, thus requiring no additional graphene source [32]. The LIG microstructure can be varied by adjusting the dots per inch (DPI) and power of the laser, which determine the conductivity of the LIG as well as the transferability of the LIG microstructure onto the tacky prepreg surface. To ensure clean transfer and sufficient prepreg conductivity, 14% power and 400 DPI were used for the purpose of this work which resulted in a porous graphitic layer approximately 100–110 μm thick. Following the laser treatment, the LIG was transferred to the surface of the unidirectional fiberglass prepreg (CYCOM® E773) using a constant pressure rolling process (figure 1(b)) during which the LIG is removed from the polyimide tape. To assist the transfer process, the prepregs were slightly heated to a temperature of 80 °C which increases the adhesion between the matrix of the prepreg and the LIG microstructure. Following the transfer of the LIG from the polyimide tape to the prepreg surface, a hot press was used to combine the LIG-coated prepregs under vacuum at 121 °C and 100 psi for 2 h. The described method was used to fabricate three separate composite plates for tensile testing, three-point bend testing, and two-dimensional damage localization of a plate. The composites for both tensile and flexural loading were comprised of three plies of fiberglass prepreg stacked at [45/-45/45]°, while the composites used for two-dimensional localization of a hole were made up of two plies of fiberglass prepreg stacked at [0/90]° (figure 1(c)). Once the composites were fully cured, the samples were cut to the desired size, and wire leads (33-gauge copper wire) were attached directly to the LIG surface using silver paint and epoxy.

The LIG interlayer was imaged using a scanning electron microscope to evaluate the microstructure both on the polyimide tape following the laser treatment, and after the transfer to the fiberglass prepreg and subsequent curing. From the images of the LIG on the polyimide (figure 1(a) callout), the LIG surface is comprised of porous individual bundles of entangled thin graphitic fibers. As stated previously, this morphology is determined by the pulsing density and power of the CO_2 laser used for the LIG process. The bundled microstructure shown in figure 1(a) is preferable both for transfer to the fiberglass prepreg matrix and high final conductivity. Subsequent to the transfer of the LIG to the fiberglass prepreg, the prepreg was cured, according to the parameters recommended by the manufacturer, resulting in the infusion of the matrix through the porous LIG structures, consequently integrating the LIG within the final composite (figure 1(b) callout). Due to the location of the LIG between reinforcing fiberglass plies, it forms an interlayer within the supporting matrix. It should be noted that since the LIG is transferred to the surface of the prepreg, any issues with dispersion or agglomeration, such as those experienced with CNTs, are fully avoided. Instead, the LIG is directly embedded within the matrix, which is then cured in place around the LIG microstructure. The addition of the LIG in the interply region of the composite results in maintained interlaminar properties, no measurable change in composite thickness, and no changes to the cure of the composite [41].

2.2. In situ localization during tensile testing

The *in situ* localization of composite failure under tension was evaluated by loading the previously described tensile specimens in a tensile test per ASTM standard D3039. Prior to testing, each sample was cut to dimensions of 0.6–0.75 inches in width and 5 inches in length, and silver paint was used to divide the specimen length into four quadrants with two additional silver paint lines at each end for current to be applied along the length of the specimen (figure 2). It can be noted that additional width was added beyond 0.5 inches to allow small slits to be cut into each side of the composite to predetermine the location of damage prior to testing. Four samples in total were tested with the damage initiated in each of the four quadrants to establish the ability of the LIG to localize damage throughout the length of the beam. Using the outermost silver paint lines, 5 mA of direct current was applied through the length of the composite using a BK Precision® model 9130 triple programmable DC power supply throughout the duration of the test. The resultant voltage across each of the four quadrants was simultaneously measured with a NI

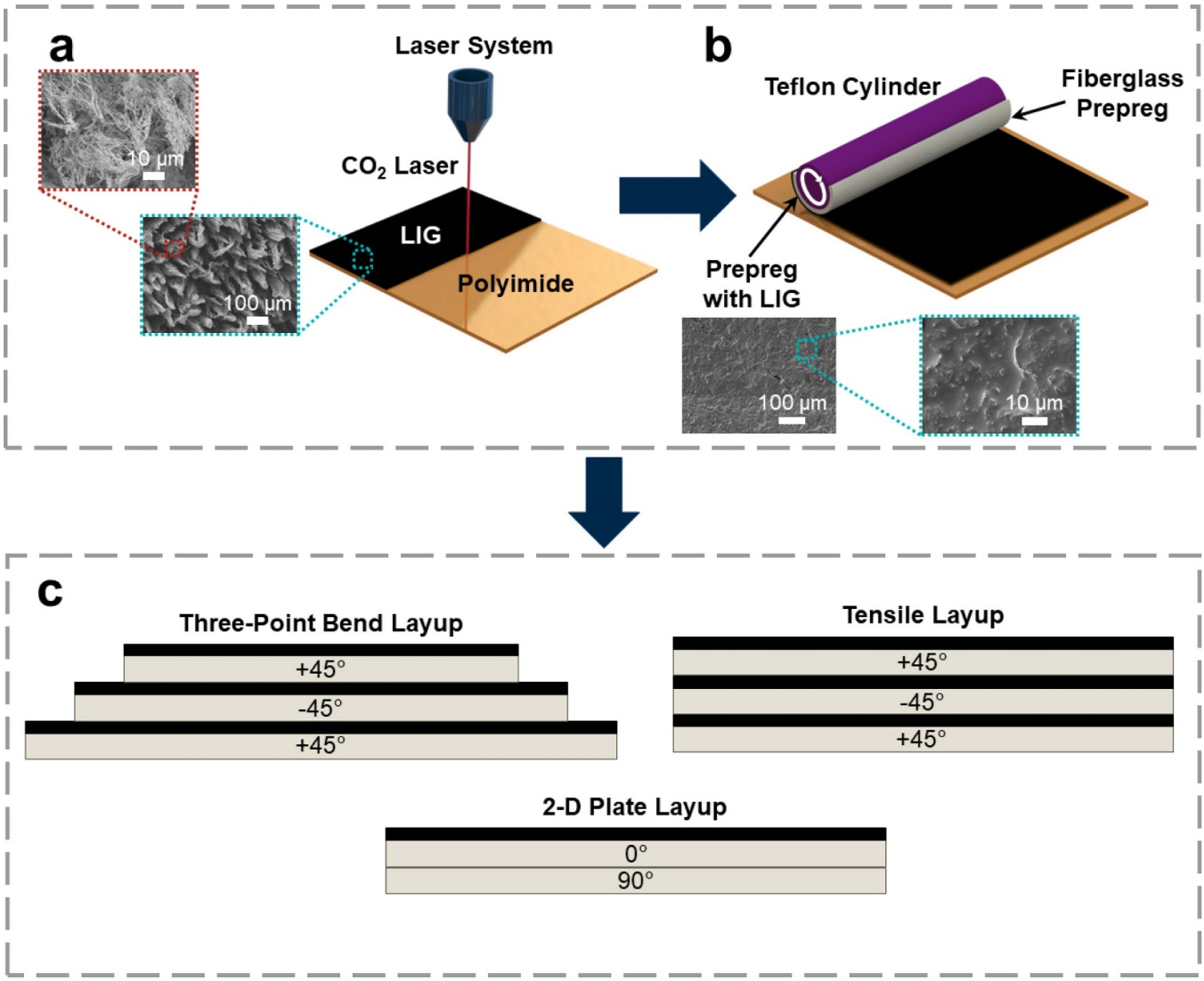

Figure 1. (a) Schematic showing the LIG fabrication. (b) Schematic of LIG transfer process onto fiberglass prepreg. (c) Stacking sequences of final composites for respective mechanical testing.

4431 data acquisition system. To predetermine the location of the majority of the damage within the sample and the resultant ultimate failure, small notches were cut into the sides of the sample in only one quadrant. A schematic of a tensile test sample with damage initiated in quadrant 1 can be seen in figure 2.

2.3. In situ localization through thickness during three-point bend testing

In addition to *in situ* tensile localization, *in situ* localization of fracture and inter-ply delamination was evaluated using mechanical testing via flexural loading in a three-point bend configuration. The three-point bend samples were designed in such a manner that the ply lengths were staggered in order to easily attach the wire leads to both ends of each individual ply as illustrated in figures 3(a) and (b). To reduce the electrical conductivity between the three LIG interlayers and ensure each measurement accurately reflected the intended ply, a small amount of additional quick-cure epoxy (Loctite® Epoxy Instant Mix™ 5 min) was placed at the edges of each ply prior to curing the composite to inhibit the flow of graphene around the edges. The offset three-ply samples were loaded with a span to thickness ratio of 32:1 as per ASTM standard D7264, using the thickness of the three-ply section of the composite specimen. In order to take multiple simultaneous measurements using the four-probe resistance measurement technique, four wire leads were attached to each ply of the specimen as illustrated in figure 3(a). The outermost wire leads on each ply were used to apply current through the ply, while the innermost wire leads were used to measure the corresponding voltage across each ply. In summary, the resulting data set contains three separate resistance measurements, corresponding to each ply. The samples were tested in two configurations: the LIG interlayers facing downward (tension configuration) shown in figure 3(c), and the LIG interlayers facing upward (compression configuration) shown in figure 3(d). This concept is discussed more fully

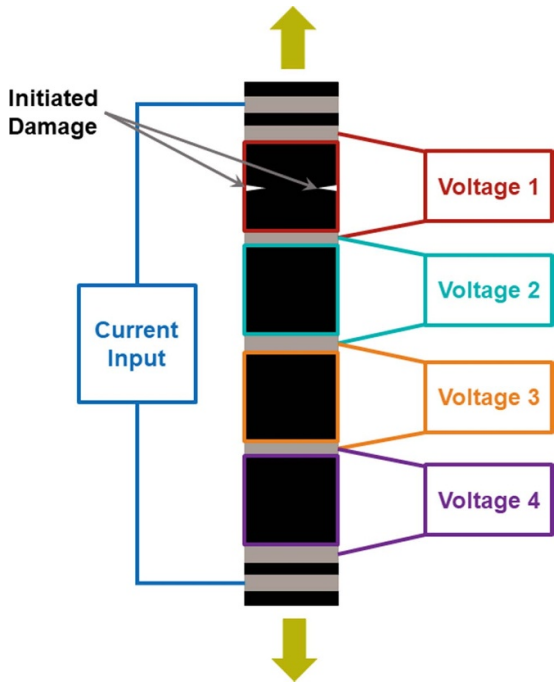

Figure 2. Schematic of current application and voltage measurements during tensile test.

elsewhere [41]. Three samples were tested in each configuration to confirm the repeatability of the damage localization capabilities of the LIG.

2.4. Two-dimensional ex-situ localization

Square samples comprised of a single layer of LIG coated fiberglass combined with one additional layer of neat fiberglass prepreg were used to investigate the potential of the LIG for two-dimensional damage localization using the normalized resistance change approach. The two two-ply LIG-coated fiberglass composites were cut to square dimensions of approximately 70 mm by 70 mm and 85 mm by 85 mm, and wire leads were attached at ∼1 cm intervals along each edge of the composite plates as shown in figures 4(a) and (e). Prior to initiating damage to the composite, several initial resistance measurements were then taken using an Agilent model 34 401 A digital multimeter. To accurately locate the position of the damage, these resistance measurements were taken in multiple configurations: horizontally and vertically across the plate (figure 4(c)), and diagonally across the plate in two directions (figures 4(b) and (d)), similar to damage localization methods using the normalized resistance change method discussed in the literature [29, 42]. Each resistance value between two points was obtained with the current sourced in both directions, and the results were averaged between the two measurements. After the baseline measurements were recorded, a hole was drilled at an arbitrary position in the plate, and final resistance measurements were collected using the same methodology previously employed. The relative percent change in resistance between the final and initial measurements was then evaluated to locate the position of the damage in reference to the plate.

3. Results and discussion

3.1. In situ damage localization during tensile testing

To initiate damage in a specific quadrant of the sample during tensile testing, small slits were cut into the sides of the sample in the desired quadrant and the change in resistance was simultaneously measured from all four quadrants using the four-probe method. Prior to testing, each quadrant had an initial resistance between approximately 115–250 Ω, and the quadrant with the damage initiation did not show a significantly different initial resistance in comparison to the other quadrants. Figures 5(a)–(e) show the applied load and percent change in resistance for all four quadrants of a sample with damage initiated in the first quadrant. From figure 5(b), the final percent increase in electrical resistance in the damaged quadrant is greater than 900%, while the relatively undamaged quadrants show only a small change at catastrophic failure. The significant change in the damaged quadrant is attributed to the complete separation between the positive and negative current connections at failure due to crack propagation. Prior to catastrophic failure, quadrant one also shows a higher rate of increasing resistance relative to the other three quadrants as a result of the propagating crack and increased strain due to the initial slits cut into the sides of the sample. This measured increase in resistance is a result of the increased separation between conductive contacts in the LIG interlayer within the specimen. As the sample is strained, the fibrous LIG decreases in conductivity as a result of the inherent piezoresistivity, while permanent separations, due to the physical separation in the LIG interlayers, result from delamination and fiber failure. Since this occurs predominantly in the first quadrant, this is the location of the most significant change in resistance. As an alternative example, the sample represented by the schematic on the right and the data in figures 5(f)–(j) had damage initiated in the fourth quadrant. Similar to the previous sample, the three relatively undamaged quadrants show a negligible change in electrical resistance while the fourth quadrant, which experienced significant damage and strain, showed a significantly higher increase in resistance with the final value reaching almost 400%. Once again, significant damage resulted in the physical separation of the conductive carbon-carbon contacts within the LIG interlayer leading to the observed increase in resistance. Although the specific value is lower than that of the previously discussed example, the relative increase exceeds any reasonable threshold indicating significant damage, thus signifying that the physical separation within the LIG interlayers is far greater in the damaged quadrant. It can be noted that the results shown in figure 5 are representative of all of the samples tested. In each case, regardless of the damage location, significantly higher changes in resistance were observed from the damage quadrant. Therefore, the samples with LIG are conclusively able to provide information which enables the determination of the damage location in one-dimension *in situ*. It can be noted that if additional linear

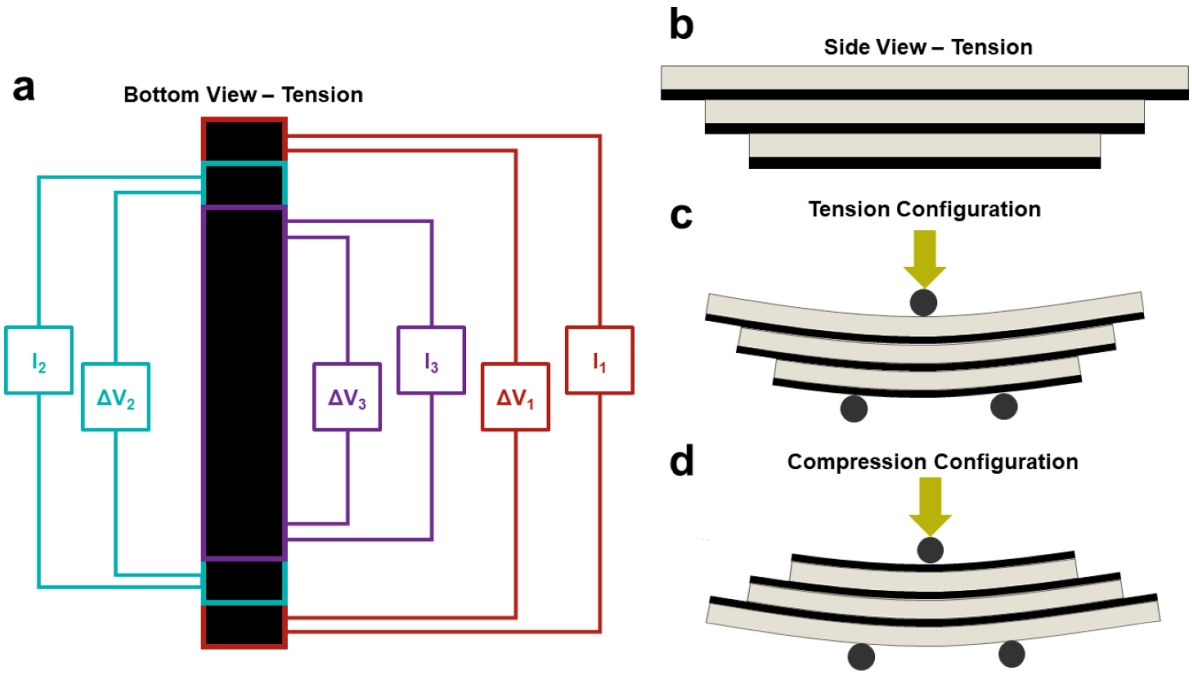

Figure 3. (a) Schematic of bottom view of tension configuration prior to flexural loading. (b) Schematic of side view of tension configuration prior to flexural loading. (c) Schematic of tension configuration during three-point bend testing. (d) Schematic of compression configuration during three-point bend testing.

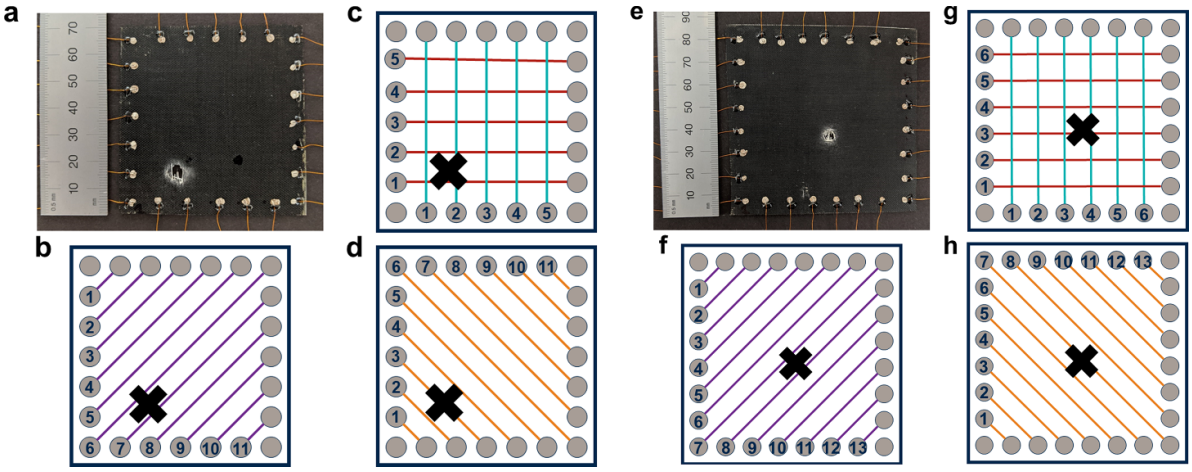

Figure 4. (a) Image of sample 1 with offset hole. (b) +45° diagonal, (c) across (horizontal and vertical), and (d) −45° diagonal current path measurements for sample 1. (e) Image of sample 2 with approximately central hole. (f) +45° diagonal, (c) across (horizontal and vertical), and (d) −45° diagonal current path measurements for sample 2.

resolution were needed for a specific application, increasing the spatial frequency of the measurements along the length of the sample would provide improved dimensional accuracy when localizing damage.

3.2. In situ localization during three-point bend testing

Flexural loading was used to evaluate the performance of the LIG composites in sensing the location of damage through the thickness of the composite. As a result of the three-point bend loading, the composite samples in this work experienced a combination of multiple significant types of damage including: interply delamination, fiber-matrix debonding, and fiber fracture resulting in fracture of one ply. Images of these types of damage within the samples taken using an optical microscope are shown in figures 6(b) and (h) for the tension and compression samples, respectively. By measuring the change in resistance of each ply individually using the four-probe technique, the extent to which each ply was involved or affected by the damage was determined. To evaluate the effect of the LIG orientation on the damage localization ability, the samples with LIG were tested in two separate orientations: the LIG surfaces oriented toward the bottom (tension dominant) and the LIG surfaces oriented toward the top

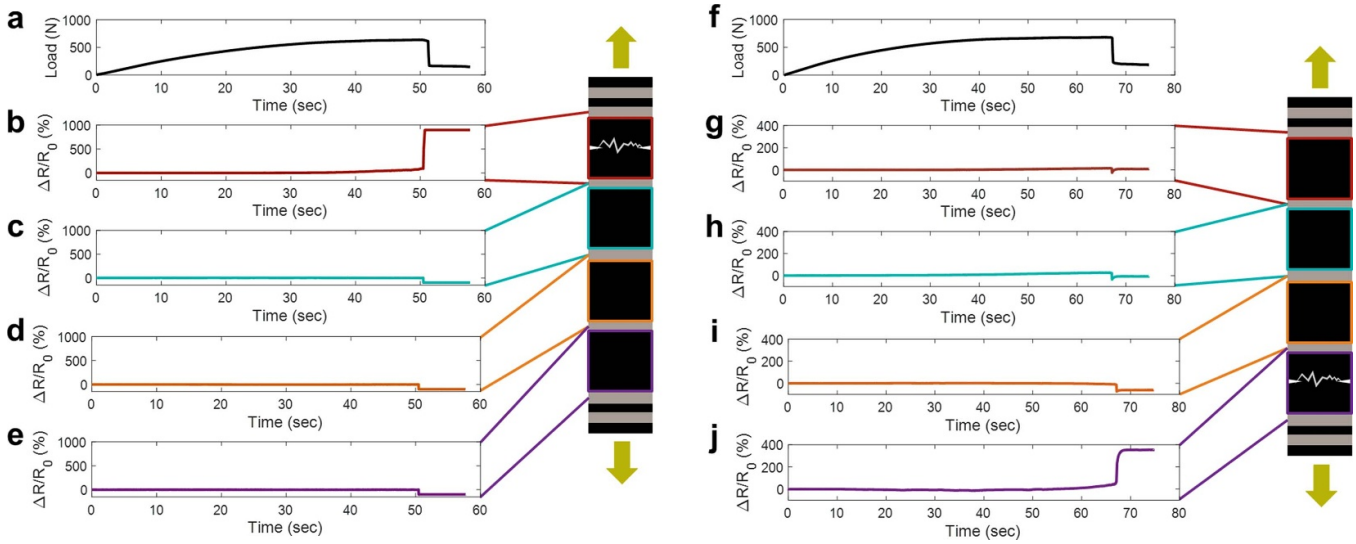

Figure 5. (a) Load, (b) change in resistance in first quadrant, (c) change in resistance in second quadrant, (d) change in resistance in third quadrant, and (d) change in resistance in fourth quadrant for tensile sample that broke in the first quadrant. (f) Load, (g) change in resistance in first quadrant, (h) change in resistance in second quadrant, (i) change in resistance in third quadrant, and (j) change in resistance in fourth quadrant for tensile sample that broke in the fourth quadrant.

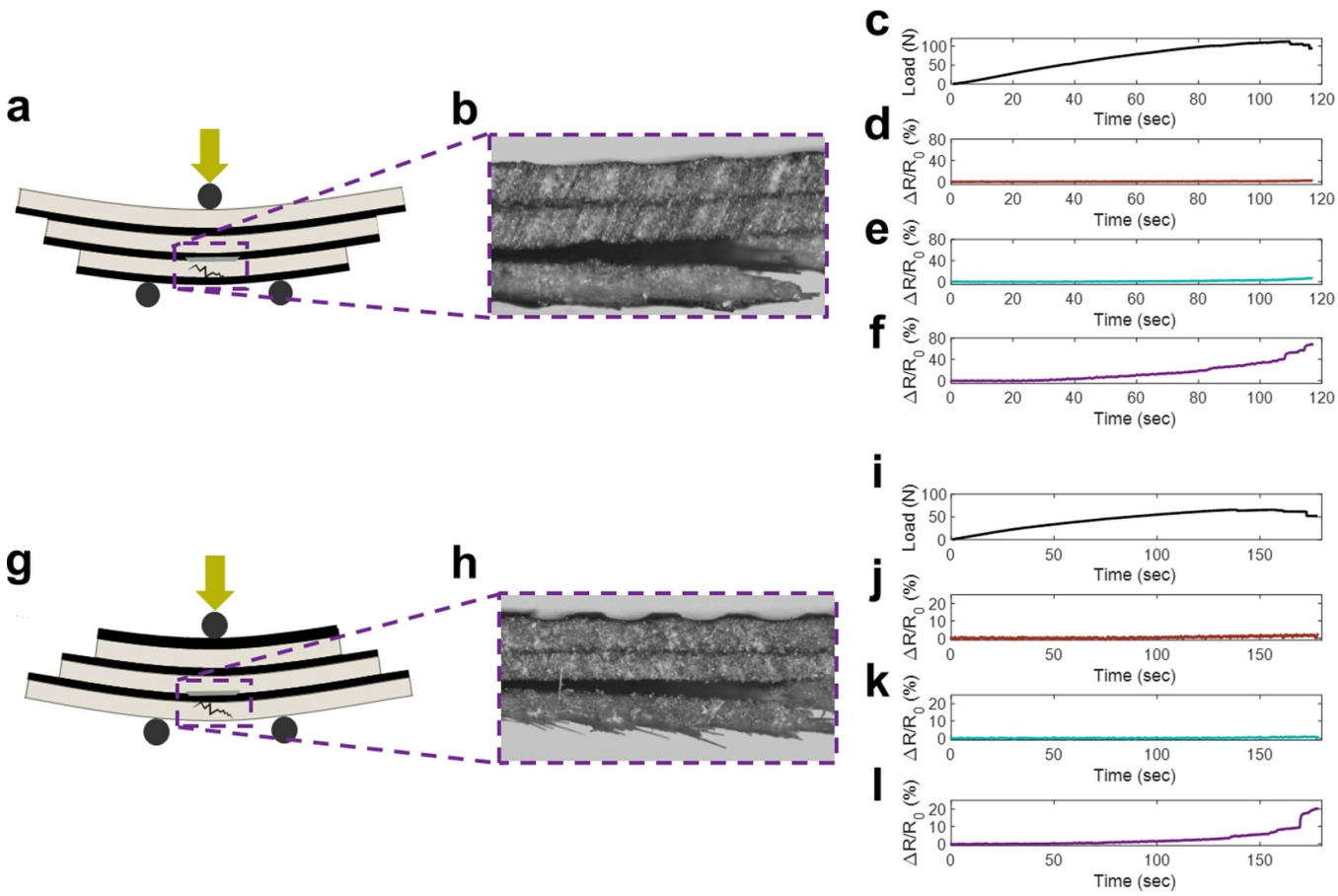

Figure 6. (a) Schematic of tension configuration and damage. (b) Optical microscope image of damage to bottom ply. (c) Applied load, (d) percent change in resistance of top ply, (e) percent change in resistance of center ply, and (f) percent change in resistance of bottom ply for one sample in the tension configuration during three-point bend testing. (g) Schematic of compression configuration and damage. (h) Optical microscope image of damage to bottom ply. (i) Applied load, (j) percent change in resistance of top ply, (k) percent change in resistance of center ply, and (l) percent change in resistance of bottom ply for one sample in the tension configuration during three-point bend testing.

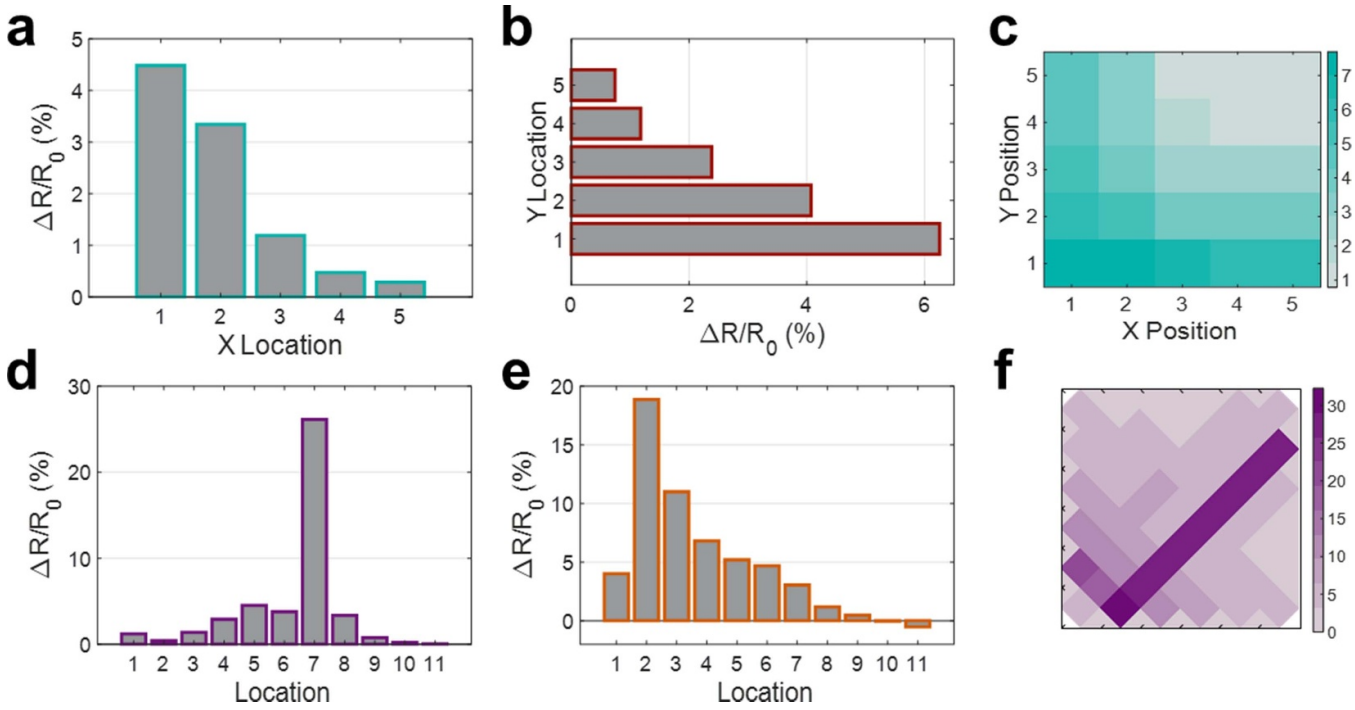

Figure 7. (a) Sample 1% change in resistance versus *x*-axis location. (b) Sample 1% change in resistance versus *y*-axis location. (c) Sample 1% change in resistance intensity map from across measurements. (d) Sample 1% change in resistance from $+45^{\circ}$ diagonal measurements. (e) Sample 1% change in resistance from -45° diagonal measurements. (f) Sample 1% change in resistance intensity map from diagonal measurements.

(compression dominant) as represented in figures 3(c) and (d), respectively. Due to the extreme separation in the bottom LIG interlayer during ply fracture in both configurations, a corresponding increase in resistance of ∼80% (figure 6(f)) in the tension configuration and ∼20% (figure 6(l)) in the compression configuration can be observed in the measurements across the damaged lamina. Additionally, a relatively small, but still significant increase in resistance (<20% in the tension configuration and <5% in the compression configuration) can be observed in the center ply which delaminated (figures 6(e) and (k)). A comparison of the percent change in electrical resistance of each ply in the tension configuration to the sample in the compression configuration indicates a smaller percent change in conductivity in each ply in the compression configuration. This is due to the fact that the LIG experiences higher strain in the tension configuration due to the location of the LIG at the point of higher positive stress. As the LIG experiences positive strain, a large degree of separation occurs within each LIG interlayer resulting in increased electrical resistance. In contrast, the LIG on the bottom surface of the sample in the compression configuration is subjected to less positive stress which causes a lower increase in resistance. However, as the sample experiences significant fracture and delamination (figures 6(b) and (h)), the physical separation of the LIG interlayers results in a relatively large increase in resistance in both cases. By examining the relative changes in conductivity in each sample individually, it is clear that the ply at the bottom which showed delamination and fracture exhibited a significantly larger change in conductivity in comparison to the plies which experienced minimal damage in both the tension and compression configurations. Consequently, the samples with LIG are capable of locating the presence of damage through the thickness during flexural loading regardless of LIG orientation. Furthermore, it should be noted that the reported results are again reflective of the entirety of the samples tested, and the location of damage was consistently determined by increased changes in resistance from the ply which sustained the majority of the flexural damage.

3.3. *In-plane damage localization*

The two-dimensional localization of damage in fiberglass composites with an LIG interlayer was experimentally investigated by drilling a hole in two composite plates at various locations and taking the resistance measurements before and after damage. For greater hole localization accuracy, resistance measurements were obtained with varying current paths: across (figures 4(c) and (g)) and diagonal (figures 4(b), (d), (f) and (h)). For reference, the initial resistance values across each plate fell within the range of ∼170–370 Ω, while the diagonal initial resistance values fell within the slightly larger range of ∼70–440 Ω due to the difference in distance between nodes. The holes were drilled at two different locations on the two different plates to evaluate relative differences in the localization accuracy with respect to damage location. On sample 1 the hole was at an offset location closer to the corner (figure 4(a)), while, the hole in sample 2 was located closer to the center of the plate (figure 4(e)). The resulting percent change in electrical resistance in sample 1 from the vertical and horizontal measurements are shown in figures 7(a) and

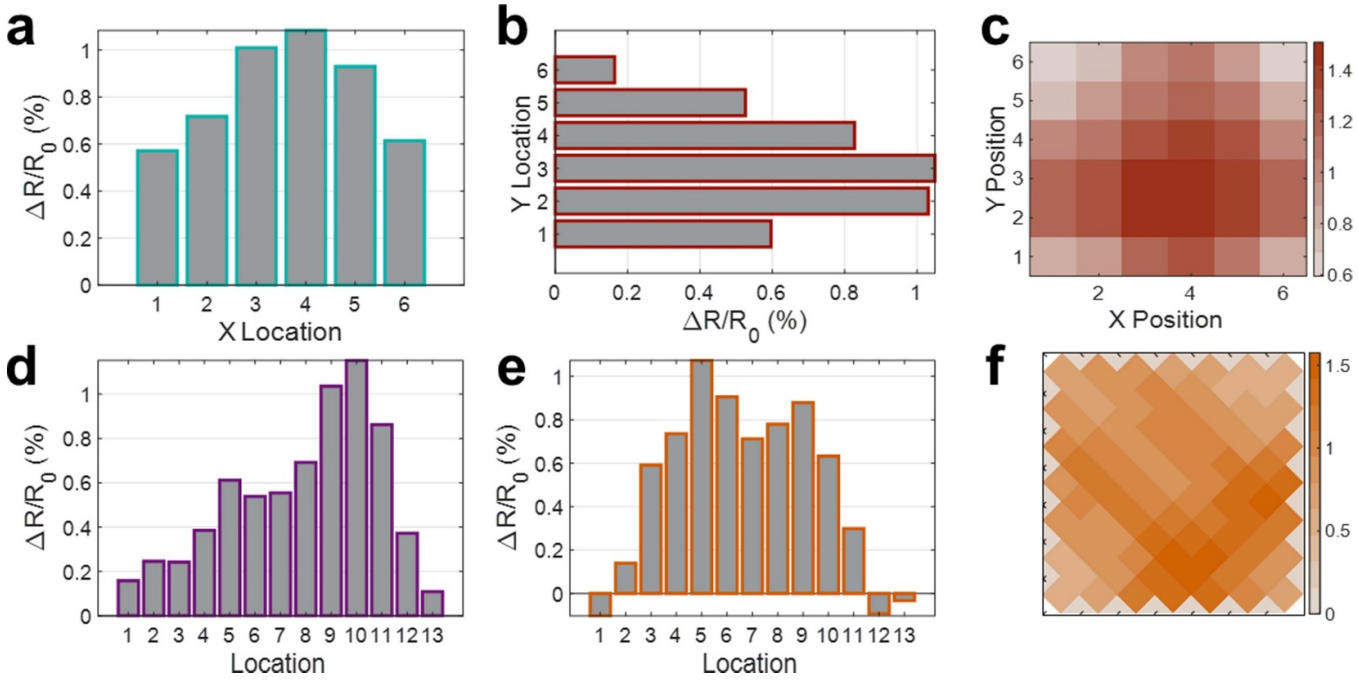

Figure 8. (a) Sample 2% change in resistance versus x-axis location. (b) Sample 2% change in resistance versus y-axis location. (c) Sample 2% change in resistance intensity map from across measurements. (d) Sample 2% change in resistance from $+45^{\circ}$ diagonal measurements. (e) Sample 2% change in resistance from -45° diagonal measurements. (f) Sample 2% change in resistance intensity map from diagonal measurements.

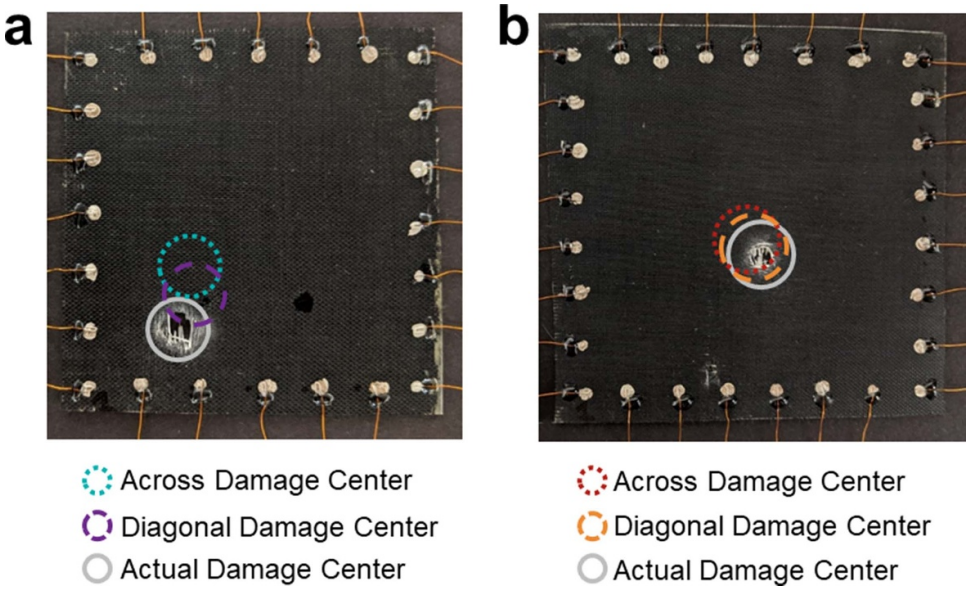

Figure 9. (a) Sample 1 damage center calculated from across and diagonal measurements compared to actual damage center. (b) Sample 2 damage center calculated from across and diagonal measurements compared to actual damage center.

(b), respectively. These measurements are then used to generate the resistance change intensity map shown in figure 7(c). For further analysis, the diagonal measurements taken across sample 1 at -45° and $+45^{\circ}$ from the horizontal are shown in figures 7(d) and (e), respectively, while the intensity map generated from the combination of both diagonal measurements is shown in figure 7(f). The visual evaluation of the difference in conductivity changes displayed in the mentioned figures conclusively shows that the percent change in resistance is significantly higher in the measurements whose paths cross over the damage. Furthermore, the point of highest percent change in each reconstructed intensity map clearly coincides with the grid point where the damage occurred on the sample itself. This is intuitive as the entirely nonconductive hole replaces LIG which provides a conductive pathway throughout the area of the composite. Thus a large loss of

Table 1. Actual versus calculated damage coordinate for both sample 1 and sample 2.

	Sample 1		*Sample 2*	
	Actual	Calculated	Actual	Calculated
x-coordinate	1.6	1.8	3.9	3.6
y-coordinate	1.0	2.0	2.7	3.0
Distance from origin	1.9	2.7	4.7	4.7
$+45^\circ$ Diagonal	6.6	6.3	8.2	7.9
-45° Diagonal	2.6	3.4	6.5	6.6

conductivity is expected in the area surrounding the hole, and this is confirmed by the resistance measurements.

Similar to the first sample, an evaluation of relative changes in the electrical resistance of sample 2 allows for the determination of the general location of the damage within the plate. The resulting percent change in electrical resistance in sample 2 from the vertical and horizontal measurements are shown in figures 8(a) and (b), respectively, and the corresponding two-dimensional intensity map is then shown in figure 8(c). For additional analysis, the diagonal measurements at -45° and $+45^\circ$ from the horizontal are presented in figures 8(d) and (e), respectively, and the generated two-dimensional intensity map is seen in figure 8(f). As with the previous sample, the across measurements which correlate to the x- and y-position of the hole show the largest increase in resistance, however, the maximum percent change is smaller in magnitude than that of sample 1. Furthermore, the diagonal measurements provide a location which is less clear than the changes observed in sample 1 due to the lower overall change in conductivity. A closer comparison of the samples indicates that the resistance measurements show increased sensitivity if the damage is located closer to the measurement nodes. In the case of an offset hole, the nonconductive area is closer to the current source or sink used to measure the electrical resistance; this is expected to cause a greater disturbance in the measured conductivity. Whereas if the hole is located toward the center of the composite, the conductive area surrounding the defect provides some compensation, thus decreasing the sensitivity of the measurement. Overall, the measurements from sample 2 assist in narrowing the region of damage within the plate, although a more specific location of the hole is not as evident from a visual comparison of the measurements and the two-dimensional intensity maps.

Although the 2D intensity maps allow for quick visual approximation of the damage location, a more robust quantitative method is needed to quickly determine where on the plate the hole is located. For this purpose, the damage center was calculated for both across and diagonal measurements using adapted center of mass equations, shown as equations (1) and (2), following the methodology of Gallo and Thostenson [29], where x_n and y_n are the x-location and the y-location of the center of the measurement, respectively, ΔR_n is the local change in resistance corresponding to the location, and ΔR_{total} is the total change in resistance of measurements taken in the same direction.

$$x_c = \frac{\sum_{i=1}^{n} x_n \Delta R_n}{\Delta R_{\text{total}}}. \quad (1)$$

$$y_c = \frac{\sum_{i=1}^{n} y_n \Delta R_n}{\Delta R_{\text{total}}}. \quad (2)$$

The calculated damage center for both across and diagonal measurements in comparison to the actual damage center for both samples are shown in figures 9(a) and (b) for sample 1 and sample 2, respectively, and a comparison of the calculated coordinates with the approximated actual coordinates of the damage are shown in table 1. In both the case of the center and offset hole, the diagonal measurements result in more accurate damage center predictions, which is attributed to the increased number of measurement points. Notably, the results also show that although the overall percent change in resistance is lower in the plate with a center hole, the calculated center of damage is closer to that of the actual damage with a maximum percent error of $\sim$0.3 cm. The improved accuracy in detecting the location of damage if it is closer to the center than the edge of the plate is similar to previous results from other works using alternative conductive nanoparticles [29], and is expected to be due to an inherent bias of the calculation toward the center of the plate. The majority of the sum of the resistance change (ΔR_{total}) is located throughout the entirety of the plate which is beyond the coordinate of the damage center thus biasing the results. Overall, the center of damage was predicted with a maximum error of $\sim$1 cm which correlates to the approximate distance between measurement points, thus indicating that an increase in node frequency has potential to increase the measurement accuracy. In summary, a combination of visual inspection of the resistance change intensity maps combined with a calculated approximation of the damage center consistently results in a relatively accurate approximation of the damage location in two dimensions, regardless of the location of the damage, using a simple and non-intrusive approach. The piezoresistive localization potential is similar to that discussed in other works investigating alternative nanomaterials, however the methods used here, as previously discussed, are notably more scalable.

4. Conclusion

This work examines the exploitation of the simple and scalable LIG process for the three-dimensional localization of damage in traditionally non-conductive fiberglass prepreg composites using piezoresistive measurements. A series of simultaneous voltage measurements stemming from a single current input allows for the localization of tensile damage *in situ* using the piezoresistance of the LIG. An adjusted method was then

employed to measure the resistance along the length of each individual ply using the four-point probe method to effectively locate delamination and ply fracture through the thickness of a fiberglass composite *in situ* during flexural loading. By utilizing three individual current sources and voltage measurements, one pair for each individual ply, the relative changes in conductivity can be used to locate the damage through the thickness. Finally, a combination of several discrete resistance measurements was used to detect the location of a hole on a two dimensional plate. Although current scattering is observed to affect the ability to accurately predict the damage center, with a maximum error value of $\sim$1 cm in the distance between the actual center and the calculated center, the general location of the damage was proven to be detectable in each case by using the piezoresistance of the LIG. Therefore, the result of this work is the effective localization of damage within fiberglass reinforced composites in three-dimensions using piezoresistive sensing methods. The processes used in this work excel in their scalability and automatability in addition to the fully integrated nature of the sensing component, thus simultaneously removing complicated processing methods and the need for external or discrete sensors for resistance-based SHM.

Acknowledgments

The authors gratefully acknowledge support from the National Science Foundation Graduate Research Fellowship Program under Grant # DGE 1256260, the National Science Foundation Grant # CMMI-1762369 and # EFRI-1935216, and the Air Force Office of Scientific Research under Grant # FA9550-16-1-0087.

ORCID iDs

LoriAnne Groo https://orcid.org/0000-0001-5296-1354
Henry Sodano https://orcid.org/0000-0001-6269-1802

References

[1] Alander P, Lassila L V, Tezvergil A and Vallittu P K 2004 *Dental Mater.* **20** 305–12
[2] Zhuang X and Yan X 2006 *Compos. Sci. Technol.* **66** 444–49
[3] Ceysson O, Salvia M and Vincent L 1996 *Scr. Mater.* **34** 8
[4] Barré S and Benzeggagh M L 1994 *Compos. Sci. Technol.* **52** 369–76
[5] Kumosa M, Hull D and Price J 1987 *J. Mater. Sci.* **22** 331–6
[6] Toyama N, Koo J-H, Oishi R, Enoki M and Kishi T 2001 *J. Mater. Sci. Lett.* **20** 1823–5
[7] Baxter M G, Pullin R, Holford K M and Evans S L 2007 *Mech. Syst. Signal Process.* **21** 1512–20
[8] Tobias A 1976 *Non-Destr. Test.* **9** 9–12
[9] Baron C and Schulte K 1988 Determination of electric resistance for in-situ determination of fibre failure in carbon fibre-reinforced plastic composites *Material-pruefung* **30** 361–66
[10] Schulte K and Baron C 1989 *Compos. Sci. Technol.* **36** 63–76
[11] Abry J C, Bochard S, Chateauminois A, Salvia M and Giraud G 1999 *Compos. Sci. Technol.* **59** 925–35
[12] Todoroki A, Tanaka Y and Shimamura Y 2002 *Compos. Sci. Technol.* **62** 1151–60
[13] McCrory J P, Al-Jumaili S K, Crivelli D, Pearson M R, Eaton M J, Featherston C A, Guagliano M, Holford K M and Pullin R 2015 *Composites* B **68** 424–30
[14] Scholey J J, Wilcox P D, Wisnom M R, Friswell M I, Pavier M and Aliha M R 2009 A generic technique for acoustic emission source location *J. Acoust. Emiss.* **27** 291–98
[15] Bar H, Bhat M and Murthy C 2005 *J. Nondestruct. Eval.* **24** 121–34
[16] Frieden J, Cugnoni J, Botsis J and Gmür T 2012 *Compos. Struct.* **94** 438–45
[17] Betz D C, Staszewski W J, Thursby G and Culshaw B 2006 *Smart Mater. Struct.* **15** 1313
[18] Betz D C, Thursby G, Culshaw B and Staszewski W J 2006 *Smart Mater. Struct.* **15** 1305
[19] Seale M D, Smith B T, Prosser W and Zalameda J N 1998 *J. Acoust. Soc. Am.* **104** 1399–403
[20] Surgeon M and Wevers M 1999 *NDT E Int.* **32** 311–22
[21] Mechraoui S-E, Laksimi A and Benmedakhene S 2012 *Compos. Struct.* **94** 1483–94
[22] Thostenson E T and Chou T-W 2006 *Adv. Mater.* **18** 2837–41
[23] Wang X, Wang S and Chung D D L 1999 *J. Mater. Sci.* **34** 2703–13
[24] Gao L, Thostenson E T, Zhang Z and Chou T-W 2009 *Adv. Funct. Mater.* **19** 123–30
[25] Gao S L, Zhuang R C, Zhang J, Liu J W and Mäder E 2010 *Adv. Funct. Mater.* **20** 1885–93
[26] Mahmood H, Vanzetti L, Bersani M and Pegoretti A 2018 *Composites* A **107** 112–23
[27] Schueler R, Joshi S P and Schulte K 2001 *Compos. Sci. Technol.* **61** 921–30
[28] Angelidis N, Khemiri N and Irving P E 2004 *Smart Mater. Struct.* **14** 147–54
[29] Gallo G J and Thostenson E T 2016 *Compos. Struct.* **141** 14–23
[30] Dai H, Gallo G J, Schumacher T and Thostenson E T 2016 *J. Nondestruct. Eval.* **35** 26
[31] Parmar K, Mahmoodi M, Park C and Park S S 2013 *Smart Mater. Struct.* **22** 075006
[32] Lin J, Peng Z, Liu Y, Ruiz-Zepeda F, Ye R, Samuel E L, Yacaman M J, Yakobson B I and Tour J M 2014 *Nat. Commun.* **5** 5714
[33] Peng Z, Ye R, Mann J A, Zakhidov D, Li Y, Smalley P R, Lin J and Tour J M 2015 *ACS Nano* **9** 5868–75
[34] Li L, Zhang J, Peng Z, Li Y, Gao C, Ji Y, Ye R, Kim N D, Zhong Q and Yang Y 2016 *Adv. Mater.* **28** 838–45
[35] Peng Z, Lin J, Ye R, Samuel E L and Tour J M 2015 *ACS Appl. Mater. Interfaces* **7** 3414–9
[36] Tao L-Q, Tian H, Liu Y, Ju Z-Y, Pang Y, Chen Y-Q, Wang D-Y, Tian X-G, Yan J-C and Deng N-Q 2017 *Nat. Commun.* **8** 14579
[37] Sun B, McCay R N, Goswami S, Xu Y, Zhang C, Ling Y, Lin J and Yan Z 2018 *Adv. Mater.* **30** 1804327
[38] Rahimi R, Ochoa M, Yu W and Ziaie B 2015 *ACS Appl. Mater. Interfaces* **7** 4463–70
[39] Luo S, Hoang P T and Liu T 2016 *Carbon* **96** 522–31
[40] Chhetry A, Sharifuzzaman M, Yoon H, Sharma S, Xuan X and Park J Y 2019 *ACS Appl. Mater. Interfaces* **11** 22531–42
[41] Groo L, Nasser J, Zhang L, Steinke K, Inman D and Sodano H 2020 *Compos. Sci. Technol.* **199** 108367
[42] Nonn S, Schagerl M, Zhao Y, Gschossmann S and Kralovec C 2018 *Compos. Sci. Technol.* **160** 231–6